Acta Pharmaceutica Sinica B 2018;8(2):261–271

Chinese Pharmaceutical Association
Institute of Materia Medica, Chinese Academy of Medical Sciences

Acta Pharmaceutica Sinica B

www.elsevier.com/locate/apsb
www.sciencedirect.com

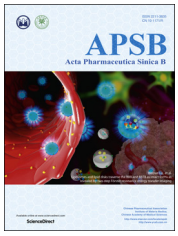

ORIGINAL ARTICLE

Liposomes and lipid disks traverse the BBB and BBTB as intact forms as revealed by two-step Förster resonance energy transfer imaging

Tongcheng Dai[a,b], **Kuan Jiang**[a], **Weiyue Lu**[a,b,c,*]

[a]*Department of Pharmaceutics, School of Pharmacy, Fudan University, and Key Laboratory of Smart Drug Delivery (Fudan University), Ministry of Education, Shanghai 201203, & State Key Laboratory of Medical Neurobiology, and Collaborative Innovation Center for Brain Science, Fudan University, Shanghai 200032, China*
[b]*State Key Laboratory of Molecular Engineering of Polymers, Fudan University, Shanghai 200433, China*
[c]*Minhang Branch, Zhongshan Hospital and Institute of Fudan-Minghang Acadimic Health System, Minghang Hospital, Fudan University, Shanghai 201199, & Institutes of Integrative Medicine of Fudan University, Shanghai 200040, China*

Received 1 November 2017; received in revised form 21 December 2017; accepted 25 December 2017

KEY WORDS

Liposomes;
Disks;
Intact form;
BBB;
BBTB;
FRET

Abstract The blood–brain barrier (BBB) and the blood–brain tumor barrier (BBTB) prevent drug and nano-drug delivery systems from entering the brain. However, ligand-mediated nano-drug delivery systems have significantly enhanced the therapeutic treatment of glioma. In this study we investigated the mechanism especially the integrity of liposomes and lipid disks while traversing the BBB and BBTB both *in vitro* and *in vivo*. Fluorophores (DiO, DiI and DiD) were loaded into liposomes and lipid disks to form Förster resonance energy transfer (FRET) nano-drug delivery systems. Using brain capillary endothelial cells as a BBB model, we show that liposomes and disks are present in the cytoplasm as their intact forms and traverse the BBB with a ratio of 0.68‰ and 1.67‰, respectively. Using human umbilical vein endothelial cells as BBTB model, liposomes and disks remained intact and traversed the BBTB with a ratio of 2.31‰ and 8.32‰ at 3 h. *Ex vivo* imaging and immunohistochemical results revealed that liposomes and disks could traverse the BBB and BBTB *in vivo* as intact forms. In conclusion, these observations explain in part the mechanism by which nano-drug delivery systems increase the therapeutic treatment of glioma.

*Corresponding author at: Department of Pharmaceutics, School of Pharmacy, Fudan University, and Key Laboratory of Smart Drug Delivery (Fudan University), Ministry of Education, Shanghai 201203, China. Tel.: +86 21 51980006; fax: +86 21 5288 0090.
E-mail address: wylu@shmu.edu.cn (Weiyue Lu).

Peer review under responsibility of Institute of Materia Medica, Chinese Academy of Medical Sciences and Chinese Pharmaceutical Association.

https://doi.org/10.1016/j.apsb.2018.01.004

1. Introduction

The blood–brain barrier (BBB), which mainly consists of capillary endothelial cells, prevents approximately 98% of small molecule drugs and nearly 100% of large molecule drugs from reaching the central nervous system[1–3]. Moreover, the blood–brain tumor barrier (BBTB), formed by specialized endothelial cells in tumors such as gliomas, prevents the transport of drugs or drug delivery systems into the cancerous tissue[4–6].

Transcytosis mediated by receptors has been utilized as an effective pathway to circumvent the BBB[7–12] and BBTB[13,14]. Nicotinic acetylcholine receptors (nAChRs) are extensively expressed on brain capillary endothelial cells and could mediate delivery of various drugs to the brain[15,16]. The peptide ^{D}CDX ($G^{D}R^{D}E^{D}I^{D}R^{D}TG^{D}R^{D}A^{D}E^{D}R^{D}W^{D}S^{D}E^{D}K^{D}F$) demonstrates excellent binding affinity to nAChRs and enables nano-drug delivery systems to target the brain[17,18]. This peptide was reported to be resistant to proteolytic degradation as compared to the ^{L}CDX peptide. Hence, ^{D}CDX was adopted as the brain-targeting ligand in this study.

As previously reported, the adhesion receptor integrin $\alpha_v\beta_3$ is overexpressed on the BBTB and on glioma cells. It plays a vital role in neovasculature formation[19,20]. The cyclic RGD peptide (cRGDyK) selectively targets integrin $\alpha_v\beta_3$ and enhances BBTB transport and tumor cell uptake[21].

Active-target ligands can significantly enhance the therapeutic efficacy of drug-loaded nano-drug delivery systems in central nervous system diseases[13,17,22,23]. It has not been established that nano-drug delivery systems can traverse BBB and BBTB as their intact forms, which could profoundly impact their ability to target diseases such as glioma.

With regard to *in vivo* distribution, inorganic nanoparticles such as iron oxide nanoparticles and gold nanoparticles can be easily measured due to their imaging properties[24]. However, tracking organic nano-drug delivery systems such as liposomes is more difficult.

Förster resonance energy transfer (FRET) is a type of fluorescence imaging which involves energy transfer from excited donors to acceptor molecules. It is widely applied in biological investigations on protein interactions, protein conformational change and enzyme activity[25]. The distance-dependent FRET signal endows it with the ability to monitor nanoparticle integrity by the loading of FRET pairs. For instance, this technique has been widely adopted to monitor the interaction of nanoparticles with the cell membrane[26] as well as polymeric nanoparticle stability in serum[27].

In this study, we designed a method of detecting the integrity of nano-drug delivery systems using DiO, DiI and DiD loaded into nano-drug delivery systems. These three fluorophores are in close proximity in nano-drug delivery systems. When excited at the DiO absorption band (488 nm), The presence or absence of a FRET signal (DiD) would indicate the integrity or dissociation of the nano-drug delivery systems. We also investigated the possibility of nano-drug delivery systems traversing BBB and BBTB as their intact forms both *in vitro* and *in vivo*.

2. Materials and methods

2.1. Materials

The fluorophores DiO, DiI and DiD were purchased from Invitrogen (Grand Island, NY, USA). 4′,6-Diamidino-2-phenylindole (DAPI) was from Roche (Basel, Switzerland). $mPEG_{2000}$–DSPE, HSPC (hydrogenated soy phosphatidylcholine) and POPC (1-palmitoyl-2-oleoyl-*sn*-glycero-3-phosphocholine) were supplied by Lipoid GmbH (Ludwigshafen, Germany). Cholesterol was purchased from Sinopharm Chemical Reagent Co., Ltd. (Shanghai, China). Mal–PEG_{3400}–DSPE was provided by Laysan Bio Co. (Arab, AL, USA). EBM-2 was from Lonza (Visp, Switzerland).

U87 (human glioblastoma cells) and HUVECs (human umbilical vein endothelial cells) were provided by Shanghai Institute of Cell Biology. Both cell lines were cultured in Dulbecco's modified Eagle medium (DMEM, Gibco) containing 10% fetal bovine serum (FBS, Gibco) at 37 °C in a humidified atmosphere containing 5% CO_2. Male ICR mice and BALB/c nude mice of 6–8 week age were supplied by Shanghai SLAC laboratory animal Co., Ltd. (Shanghai, China). All animal experiments were performed in accordance with guidelines approved by the ethics committee of Fudan University, Shanghai, China.

2.2. Synthesis of peptide and functional materials

The peptides $G^{D}R^{D}E^{D}I^{D}R^{D}TG^{D}R^{D}A^{D}E^{D}R^{D}W^{D}S^{D}E^{D}K^{D}F$ (CDX) and c(RGDyK) (RGD) were synthesized by GL Biochem (Shanghai) Ltd. CDX–PEG_{3400}–DSPE was synthesized *via* the sulfhydryl-maleimide coupling method. In short, 20 mg of maleimide–PEG_{3400}–DSPE (mal–PEG_{3400}–DSPE) was dissolved in *N*,*N*-dimethylformamide (DMF) and 10 mg of CDX–Cys was dissolved in phosphate buffer (0.1 mol/L, pH = 7.4). The solutions were mixed and stirred at room temperature for 2 h. Excessive CDX–Cys was removed by dialysis against distilled water. The solution was lyophilized to obtain pure CDX–PEG_{3400}–DSPE. RGD–PEG_{3400}–DSPE was also prepared according to the above method. Both were characterized by ^{1}H NMR.

2.3. Preparation and characterization of nano-drug delivery systems

2.3.1. Preparation of liposomes

Liposomes loaded with 3D (DiO, DiI and DiD), including liposomes without any targeting moiety (LS/3D), liposomes decorated with CDX (CDX–LS/3D), liposomes modified with RGD (RGD–LS/3D) and those modified with both CDX and RGD (CDX+RGD–LS/3D), were prepared by the thin-film hydration and extrusion method[28]. For blank liposomes, the ratio of components is shown in Table 1, and were dissolved in $CHCl_3$ solution and then rotary evaporated to form a thin film. The dried lipid film was subsequently hydrated in saline at 65 °C for 2 h. The lipid dispersion then was extruded through a series of polycarbonate membranes with pore size ranging from 200 to 50 nm using an Avanti Mini Extruder (Avanti Polar Lipids).

2.3.2. Preparation of disks

Lipid disks loaded with DiO, DiI and DiD, including disks without any targeting moiety (Disks/3D), disks decorated with CDX (CDX–Disks/3D), disks modified with RGD (RGD–Disks/3D) and those modified with both CDX and RGD (CDX+RGD–Disks/3D), were prepared by the thin-film hydration and ultrasound method[29]. The ratio of components in the different forms of blank disks are presented in Table 2. A mixture of the indicated materials in chloroform was rotary-evaporated to form a thin film. The lipid film was dried under vacuum overnight and hydrated in phosphate-buffered saline (PBS) for 1 h at 37 °C. Disks were subsequently

Table 1 The molar ratio of components in different forms of liposomes.

Component	LS/3D	CDX–LS/3D	RGD–LS/3D	CDX+RGD–LS/3D
HSPC	52	52	52	52
Cholesterol	43	43	43	43
$mPEG_{2000}$–DSPE	5	3	4	2
CDX–PEG_{3400}–DSPE	0	2	0	2
RGD–PEG_{3400}–DSPE	0	0	1	1

Table 2 The molar ratio of components in different forms of disks.

Component	Disks/3D	CDX–Disks/3D	RGD–Disks/3D	CDX+RGD–Disks/3D
POPC	35	35	35	35
Cholesterol	40	40	40	40
$mPEG_{2000}$–DSPE	25	23	23	23
CDX–PEG_{3400}–DSPE	0	2	0	1
RGD–PEG_{3400}–DSPE	0	0	2	1

prepared by sonication of the hydrated solution for 30 min in an ice-bath using a JY92-II sonicator (Scientz, Ningbo, China). The resulting solution was filtered through a 0.22 μm filter to remove metal debris.

2.3.3. *Characterization of nano-drug delivery systems*

The particle size distributions of different nano-drug delivery systems were determined by the dynamic light scattering method (Nicomp™ 380ZLS, USA). Size and morphology were further investigated by transmission electron microscopy (TEM) and cryogenic transmission electron microscopy (Cryo-EM)[30].

2.4. *In vitro BBB modeling and BBB transport*

The BBB model was established as previously reported[31]. In brief, rat primary brain capillary endothelial cells (BCECs) were isolated and seeded into a transwell chamber coated with rat tail collagen in a 24-well plate. Transendothelial electrical resistance (TEER) was measured by an epithelial volt-Ωm (Millicel-RES, Millipore, USA) to estimate the cell monolayer integrity. Monolayers with TEER over 200 $\Omega \cdot cm^2$ were used for further experiments. BBB monolayer was incubated with LS/3D, CDX–LS/3D, Disks/3D or CDX–Disks/3D at 37 °C. Solutions collected from the lower compartment at different time points were analyzed by fluorescence spectroscopy.

2.5. *Cell uptake*

BCECs and HUVECs were seeded into confocal dishes at a density of 2×10^4 cells per well. After incubation, the culture medium was replaced with LS/3D, CDX–LS/3D, Disks/3D or CDX–Disks/3D in DMEM supplemented with 10% FBS and the cells were incubated at 37 °C for 4 h. Cells were fixed by formaldehyde and stained for nuclei by DAPI. Intracellular distribution was observed by confocal laser scanning microscope (CLSM).

2.6. *Biodistribution of nano-drug delivery systems in brain and brain tumor*

Different formulations of liposomes and disks were injected into ICR mice or tumor-bearing nude mice *via* the tail vein. After the indicated time, the mice were killed and the brain was collected for FRET imaging using a live animal imaging system (Xenogen IVIS spectrum, USA, excitation/emission, 488/680 nm).

2.7. *Immunofluorescence analysis*

Collected brains were embedded in Tissue OCT-Freeze compound and frozen by liquid nitrogen. Then they were sectioned by microtome at –20 °C into slices of 8 μm thickness, and subsequently fixed in cold acetone for 10 min at 4 °C. PBS containing 10% FBS was applied for 15 min to block nonspecific binding sites. The primary antibody of CD31 was rat anti-mouse CD31 antibody (dilution, 1:100); Alexa Fluor® 488 goat anti-rat IgG antibody was used for the secondary antibody (dilution, 1:1500). Nuclei were stained with DAPI. After each step, the sections were washed with PBS three times. The sections were analysed with a Zeiss LSM 710 NLO confocal microscope. (DAPI, excitation: 405 nm, emission: 410–450 nm; anti-CD31 antibody, excitation: 488 nm, emission: 500–540 nm; FRET, excitation: 488 nm, emission: 650–750 nm; DiD, excitation: 633 nm, emission: 650–750 nm).

3. Results

3.1. *Synthesis and characterization of CDX–PEG_{3400}–DSPE and RGD–PEG_{3400}–DSPE*

Functional materials CDX–PEG_{3400}–DSPE and RGD–PEG_{3400}–DSPE were prepared *via* sulfhydryl-maleimide coupling. In the ^1H NMR spectrum (Supplementary Information Fig. S1) of Mal–PEG_{3400}–DSPE, the characteristic peak at 6.7 ppm was from the maleimide group, which disappeared in the spectra of CDX–PEG_{3400}–DSPE and RGD–PEG_{3400}–DSPE. It suggests that the

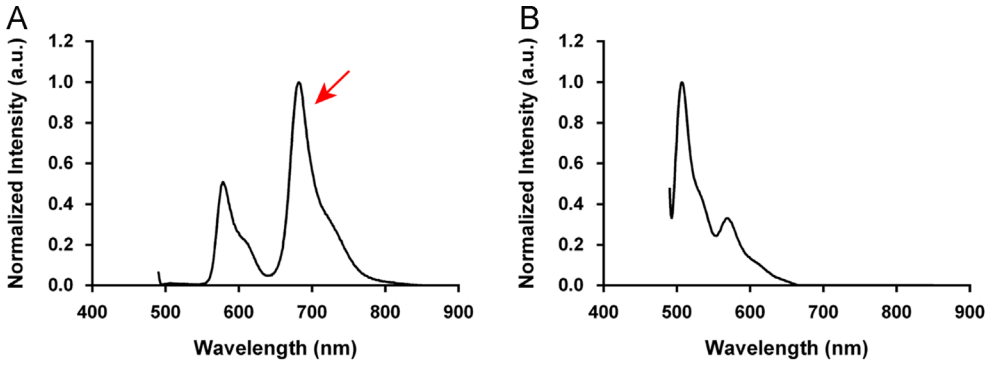

Figure 1 Fluorescence measurement of FRET pairs (DiO, DiI and DiD) encapsulated in liposomes. (A) Fluorescence spectra of liposomes/3D (excitation at 488 nm, in the DiO absorption band). Red arrow indicates DiD fluorescence attributed to the FRET effect. (B) Loss of FRET signal and DiD fluorescence upon particle dissociation in the presence of 5% Triton X-100. FRET, forster resonance energy transfer; 3D, DiO, DiI and DiD.

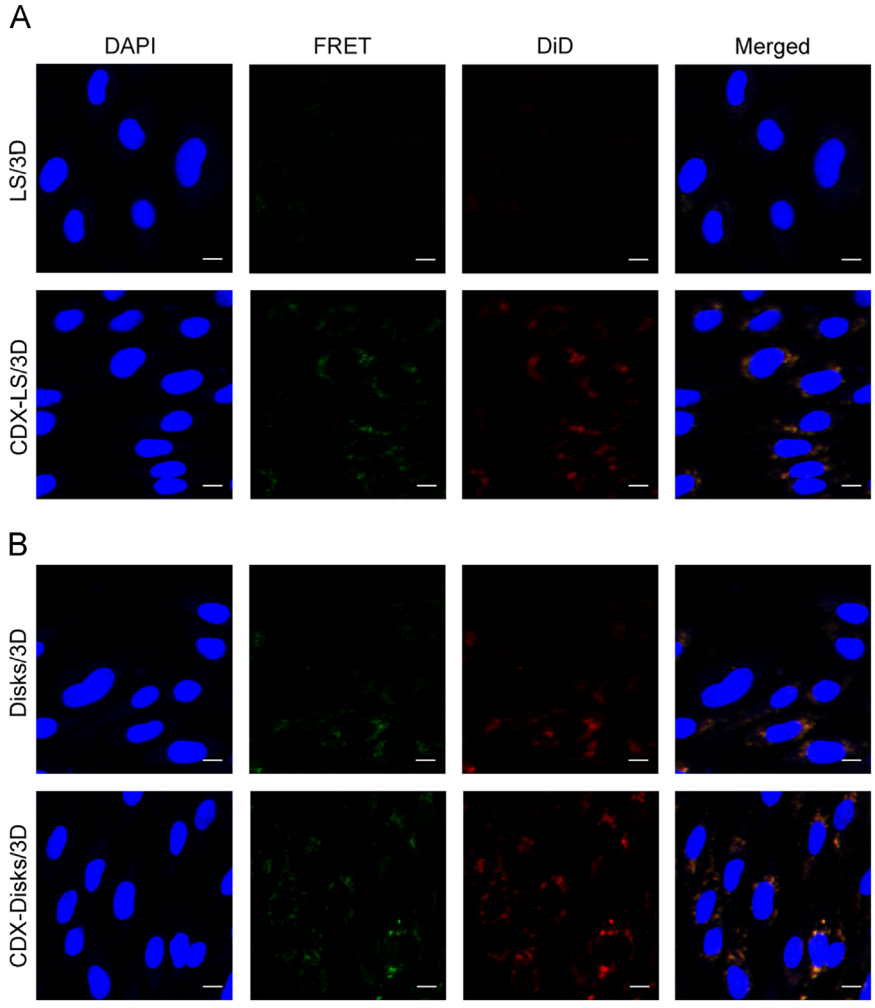

Figure 2 Cellular uptake of DiO-, DiI- and DiD-loaded liposomes or disks by BCECs. BCECs were incubated with the indicated liposome or disk formulations at 37 °C for 4 h, followed by DAPI staining. CLSM imaging was conducted to detect cellular uptake of integrated liposomes or disks. Scale bar = 10 μm. BCECs, brain capillary endothelial cells; CLSM, confocal laser scanning microscope.

thiol group of CDX–Cys and RGD–Cys had completely reacted with the maleimide group of Mal–PEG_{3400}–DSPE.

3.2. *The synthesis and characterization of FRET nano-drug delivery systems*

Highly hydrophobic dialkylcarbocyanine dyes DiO, DiI and DiD can be incorporated with efficiency >95% into the particle lipid core. DiO, DiI and DiD could efficiently interact by FRET due to the strong spectral overlap of emission and absorption wavelengths between them.

Because of the presence of FRET from DiO to DiI, DiI to DiD, an excitation at 488 nm, corresponding to the DiO excitation wavelength, produced a decrease of the DiO and an increase of the DiD emission bands respectively (Fig. 1A). Similar results were obtained with DiO, DiI and DiD loaded Disks (Supplementary Information Fig. S2).

As expected, FRET interactions between co-encapsulated donors and acceptors were disrupted when the intact nanoparticles were destroyed. For instance, when in contact with Triton-X100, DiO and DiI fluorescence was no longer transferred to DiD, resulting in the disappearance of DiD emission (Fig. 1B). The presence or disappearance of DiD fluorescence can be considered as a reliable and simple indicator of nanoparticle integrity. Similar results were discovered with DiO, DiI and DiD loaded Disks (Supplementary Information Fig. S2).

As shown in Supplementary Information Table S1, The average size of LS/3D, CDX–LS/3D, RGD–LS/3D and (CDX+RGD)–LS/3D were 95.1±1.2, 127.9±0.4, 117.9±0.4 and 132.4±0.4 nm, respectively. They had a similar polydispersity index. The zeta-potentials of LS/3D, CDX–LS/3D, RGD–LS/3D and (CDX+RGD)–LS/3D were –4.83±0.07, 2.97±0.20, –4.37±0.13 and 2.94±0.12 mV, respectively. The average size of different disk formulations varied between 67–80 nm. They also had a similar polydispersity index. The zeta-potentials of Disks/3D, CDX–Disks/3D, RGD–Disks/3D and CDX+RGD–Disks/3D were –11.3±0.06, –6.93±0.07, –7.49±0.08 and –7.22±0.05 mV, respectively. TEM was used to determine the particle shape and size of liposomes. It indicated that liposomes were spherical or near spherical with a diameter of approximately 100 nm (Supplementary Information Fig. S3), and no obvious size change was discovered upon ligand modification. Cryo-EM images demonstrated disk-shaped structures with a diameter of approximately 65 nm (Supplementary Information Fig. S4). No significant structural change was discovered upon ligand modification.

3.3. *Nano-drug delivery systems traverse the BBB in vitro as intact forms*

In order to investigate whether liposomes or disks could traverse the BBB as intact forms, BCECs were chosen as BBB model cells and were spread onto a transwell membrane to form the BBB model; it was deemed acceptable when the TEER of the monolayer was over 200 Ω·cm^2.

We first determined if nano-drug delivery systems remained intact after uptake by BCECs. CLSM imaging was used to detect intact liposomes and disks. As shown in Fig. 2, when cells were incubated with these nano-drug delivery systems for 4 h the FRET fluorescence (488 nm excitation, green) was evident in the cytoplasm, indicating that DiO, DiI and DiD were close to each other and the nano-drug delivery system remained intact when taken up by BCECs. Ligand CDX increased the intensity of FRET fluorescence, suggesting CDX enhanced the amount of intact liposomes or disks in cells. The fluorescence of DiD (633 nm excitation, red) colocalized with the FRET fluorescence, which further confirmed nano-drug delivery systems were integrated.

To investigate the efficiency of transfer across the BBB of intact nano-drug delivery systems, an *in vitro* BBB monolayer was incubated with liposomes or disks at 37 °C. Solutions collected from the lower compartment at different time points were analyzed by fluorescence spectrophotometry. As shown in Fig. 3., the percentage of intact liposomes or disks displayed a linear increase in a time-dependent fashion. CDX modification on the surface of liposomes or disks increased the percentage of intact nano-drug delivery systems traversing the BBB. After 3 h, the amount of intact nano-drug delivery systems traversing the *in vitro* BBB monolayer were 0.68‰ (CDX–LS, Fig. 3.A) and 1.67‰ (CDX–Disks, Fig. 3.B), respectively.

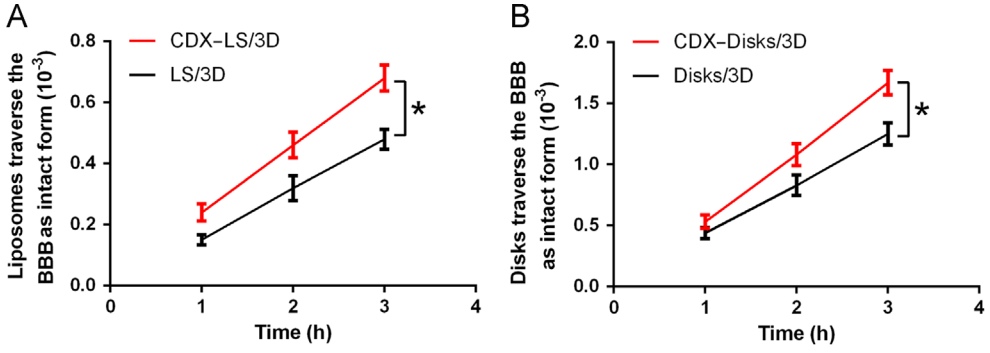

Figure 3 Transcytosis efficiency of integrated liposomes (A) and disks (B) in the *in vitro* BBB monolayer. Fluorescence spectrophotometry was conducted to detect the amount of intact liposomes and disks that crossed the BBB monolayer. Error bars represent S.D. ($n = 3$), $^{*}P<0.05$ (two-tailed Student's *t*-test). BBB, blood–brain barrier.

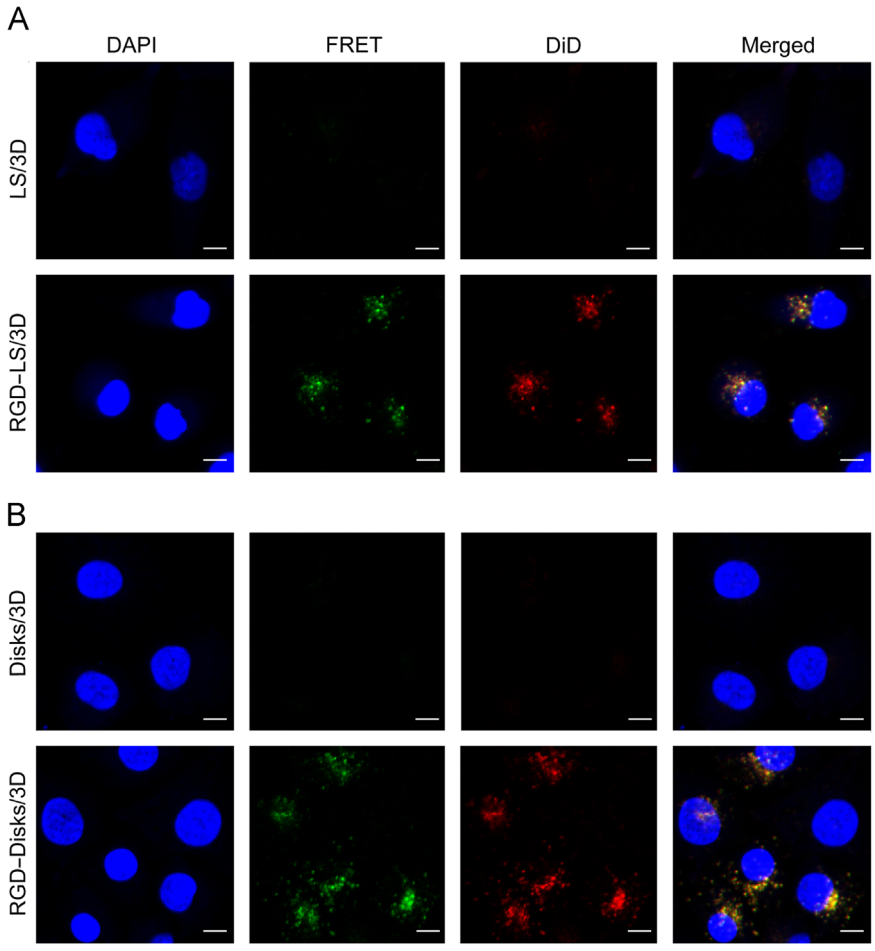

Figure 4 Cellular uptake of 3D-loaded liposomes or disks by HUVECs. HUVECs were incubated with the indicated liposome or disk formulations at 37 °C for 4 h, followed by DAPI staining. Confocal laser scanning microscope imaging was conducted to detect cellular uptake of intact liposomes or disks. Scale bar = 10 μm. HUVECs, human umbilical vein endothelial cells.

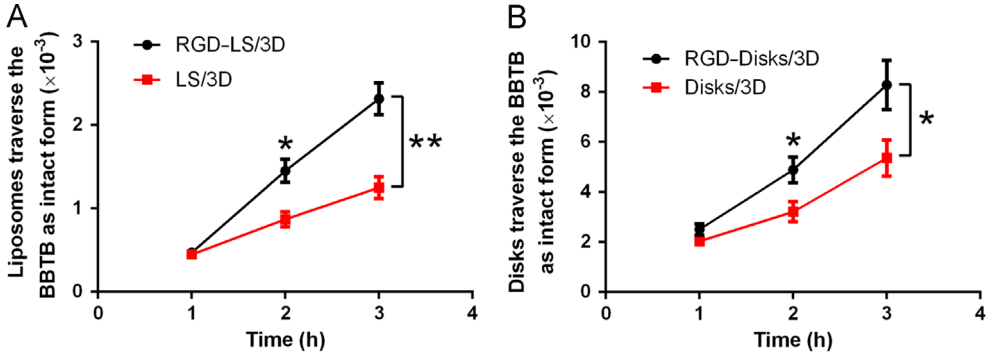

Figure 5 Transcytosis efficiency of intact liposomes (A) and disks (B) in the *in vitro* BBTB monolayer. Error bars indicate S.D. ($n = 3$). $^{**}P < 0.01$, $^{*}P < 0.05$ (two-tailed Student's *t*-test). Fluorescence spectrophotometry was used to detect the amount of integrated liposomes and disks that crossed the BBTB monolayer.

3.4. Nano-drug delivery systems traverse the BBTB in vitro as intact forms

In order to investigate whether nano-drug delivery systems (liposomes and disks) could traverse the BBTB as intact forms, HUVECs were chosen as BBTB model cells,[32,33]. and were spread onto a transwell membrane to form the BBTB model.

After nano-drug delivery systems were taken up by HUVECs, CLSM imaging was conducted to determine if they were still intact in cells. As shown in Fig. 4, when cells were incubated with liposomes or disks, the FRET fluorescence of RGD-modified groups (488 nm excitation, green) after 4 h was evident in the cytoplasm, suggesting that DiO, DiI and DiD were close to each other and the nano-drug delivery systems

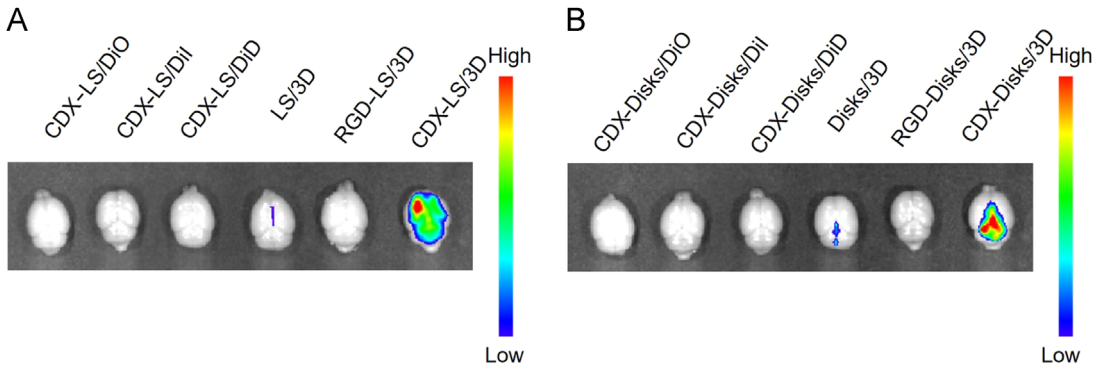

Figure 6 *Ex vivo* imaging of liposomes (A) and disks (B) in the brains of ICR mice. The excitation wavelength was 488 nm and the emission filter was 680 nm. LS, liposomes.

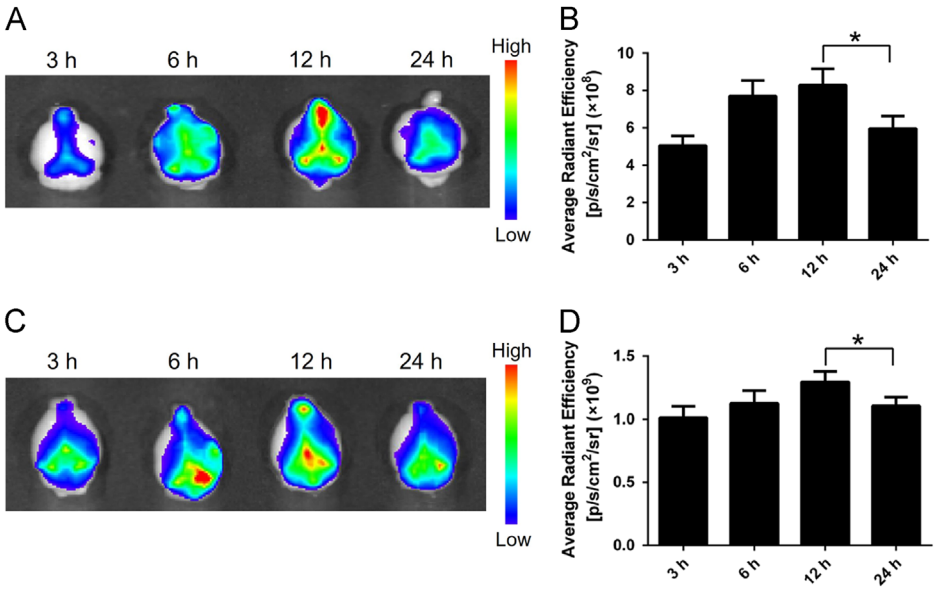

Figure 7 The *ex vivo* imaging of CDX-modified liposomes/3D (A) and disks/3D (C) in the brains of ICR mice. Error bars represent S.D. ($n = 3$), $^{*}P < 0.05$ (two-tailed Student's *t*-test). The excitation wavelength was 488 nm and the emission filter was 680 nm. (B) Semi-quantitative analysis of the fluorescence intensity of (A). (D) Semi-quantitative analysis of the fluorescence intensity of (B).

were largely intact when taken up by HUVECs. The fluorescence of DiD (633 nm excitation, red) was colocalized with the FRET fluorescence, which further verified that nano-drug delivery systems were integrated in BBTB cells.

To investigate the efficiency of transfer of integrated liposomes or disks across the BBTB, an *in vitro* BBTB monolayer was incubated with these drug delivery systems at 37 °C for various times. Solutions collected from the lower compartment at different time points were measured by fluorescence spectrophotometry. As shown in Fig. 5, the ratio of integral nano-drug delivery systems showed a linear increase in a time-dependent manner. RGD modification on the surface of liposomes or disks enhanced the amount of integrated nano-drug delivery systems. After 3 h, the amount of integrated nano-drug delivery systems in the *in vitro* BBTB monolayer cells was 2.31‰ (RGD–LS, Fig. 5.A) and 8.32‰ (RGD–Disks, Fig. 5.B), respectively.

3.5. Nano-drug delivery systems traverse the BBB in vivo as intact forms

To investigate whether nano-drug delivery systems could traverse the BBB *in vivo* as intact forms, *ex vivo* FRET fluorescence imaging was used to evaluate the biodistribution of 3D-loaded liposomes or disks in the brain of normal ICR mice. The excitation wavelength was 488 nm and the emission filter was 680 nm (FRET fluorescence). As displayed in Fig. 6A, no fluorescence signals were found in the brains treated with CDX-decorated liposomes loaded with a single fluorescent dye and with RGD-modified 3D-loaded liposomes. The LS/3D group showed a faint fluorescence signal in brain. However, there was strongly detectable FRET fluorescence in the brains of CDX–LS/3D-treated mice after 12 h, suggesting that the fluorescence signal was coming from the FRET effect and BBB target ligand CDX could significantly enhance the amount of intact liposomes in the brain. A similar trend was confirmed in the disk-treated group (Fig. 6B).

To further resolve precise localization of integrated nano-drug delivery systems within the brains of the normal ICR mice, the above mentioned brains were sectioned and stained for immunohistochemistry. The vascular endothelium-specific protein CD31 was labelled in green fluorescence with Alexa Fluor 488-conjugated anti-CD31 antibody. For FRET detection, the excitation wavelength was also set at 488 nm and the emission wavelength was 650–750 nm (FRET fluorescence, red). As presented in the

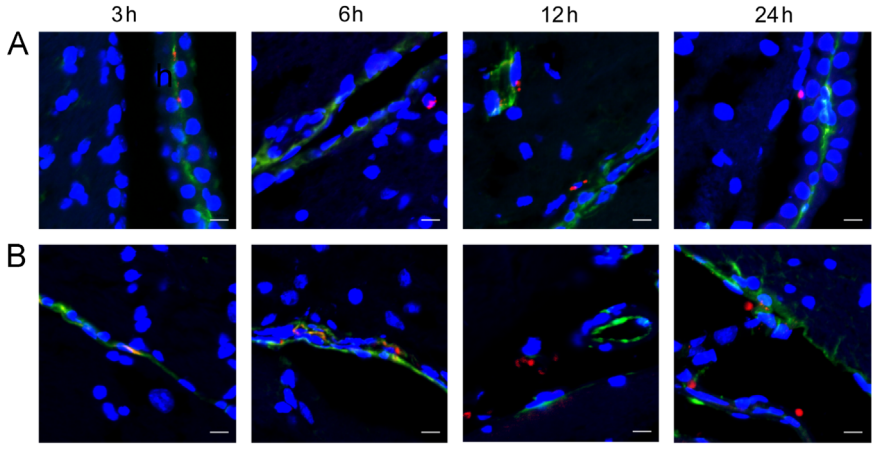

Figure 8 The localization of CDX-modified liposomes/3D (A) and disks/3D (B) in the brains of ICR mice. CD31 (green) was stained with anti-CD31 antibody. The excitation wavelength of liposomes or disks was 488 nm and the emission filter was 680 nm. Scale bar = 10 μm.

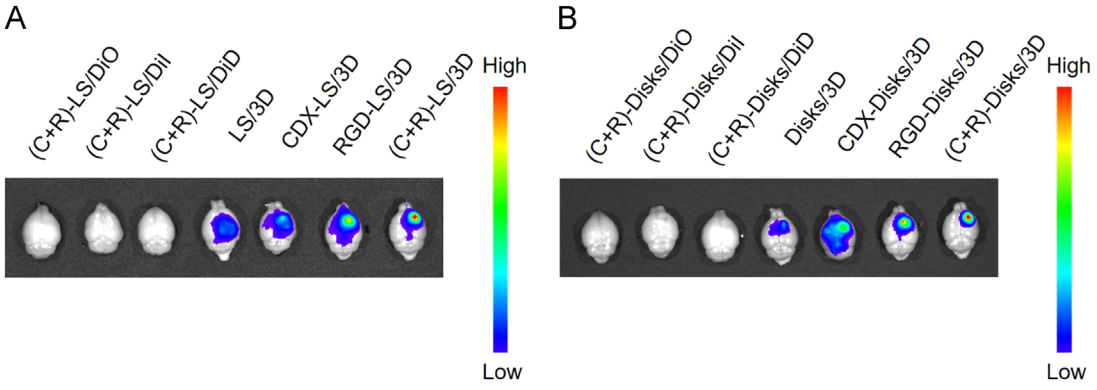

Figure 9 The *ex vivo* imaging of liposomes (A) and disks (B) in the brains of nude mice bearing an intracranial glioma 15 days post-implantation. The excitation wavelength was 488 nm and the emission filter was 680 nm. C+R, CDX+RGD.

Supplementary Information Fig. S5., nearly no FRET fluorescence signals were observed in the groups treated with CDX-decorated liposomes loaded with a single fluorescent dye and RGD-modified 3D-loaded liposomes. Conversely, CDX-functionalized liposomes loaded with 3D demonstrated visible FRET fluorescence and localized outside of blood vessels, suggesting that integral liposomes were present and had traversed the BBB *in vivo*. The microscopic results were in agreement with those of *ex vivo* imaging. To further verify that the liposomes were intact, DiD itself fluorescence was excited at 633 nm and results revealed that it colocalized with FRET fluorescence (Supplementary Information Fig. S6). This suggests that the liposomes were indeed intact. Similar results were confirmed in the groups treated with lipid disks (Supplementary Information Figs. S6 and S7).

In order to further investigate the process of intact liposomes or disks into the brain, *ex vivo* FRET fluorescence imaging was used to evaluate the biodistribution of CDX-modified 3D-loaded liposomes or disks in the brains of normal ICR mice. As shown in Fig. 7A, the amount of integrated liposomes was increased in the brain up to 12 h and gradually decreased (24 h), as quantified in Fig. 7.B. As presented in Fig. 7C and D, CDX–Disks/3D also showed a similar phenomenon in the brain.

To further inspect the process of intact nano-drug delivery systems in normal ICR mice, the brains from Fig. 7. were sectioned and stained for immunohistochemistry. At 3 h, most of the intact liposomes were still in the blood. With time it was found that the intact CDX-modified liposomes had crossed the BBB and entered the brain at 6 h and still were present at 24 h (Fig. 8A). In contrast, the CDX-modified disks slowly crossed the BBB and at 6 h most were still localized in the blood vessels (Fig. 8.B). Intact disks in the brain could be clearly detected at 12 h and were still present in the brain at 24 h.

3.6. Nano-drug delivery systems traverse the BBTB in vivo as intact forms

During the early stages, the BBB prevents nano-drug delivery systems from reaching the tumor sites. With the progression of the glioma, the BBTB appears as the main obstacle for nano-drug delivery systems.

Herein, we studied the biodistribution of various liposomes and disks containing FRET-pair dyes in nude mice bearing intracranial gliomas at 12 days after tumor implantation. Mice were killed and the brains were dissected for imaging 12 h post-injection. As shown in Fig. 9A, no fluorescence was detectable in CDX+RGD–LS loaded with a single fluorescent dye. Unmodified LS/3D rarely and randomly distributed in the brain. CDX–LS/3D was slightly distributed in the brain tumor because of its BBB targeting, while RGD–LS/3D accumulated in brain tumor more readily due to BBTB- and tumor-targeting ability. More importantly, the most significant fluorescence was in the tumor region of the group

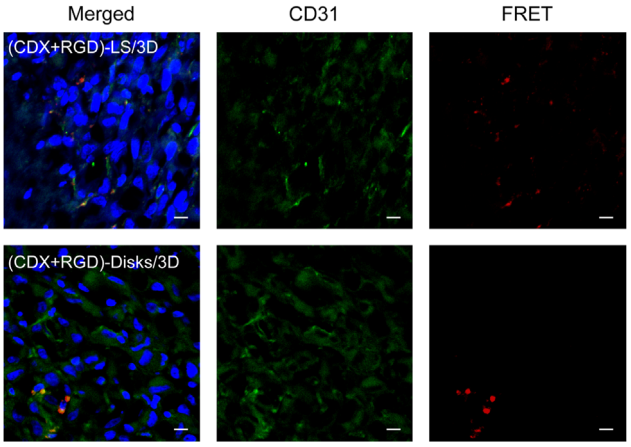

Figure 10 The distribution of liposomes and disks in the brain tumors of nude mice bearing an intracranial glioma 15 days after tumor implantation. Nuclei were stained with DAPI (blue), while green represents blood vessels (CD31 staining). For FRET fluorescence (red), the excitation wavelength was 488 nm and the emission wavelength was 650–750 nm. Scale bar = 10 μm.

treated with 3D-loaded liposomes modified with both CDX and RGD, indicating effective and precise brain tumor targeting of intact liposomes. Integrated CDX+RGD–LS could cross the BBB and BBTB and target tumor cells. Multiple barrier-targeting ability endowed intact liposomes with an effective glioma-targeting ability. Similar results also were detectable in the disk-treated group (Fig. 9B).

To further resolve precise localization of integrated nano-drug delivery systems within the brain tumor, the above mentioned brains were prepared for immunohistochemical staining. As shown in Supplementary Information Fig. S8, nearly no FRET fluorescence signals were observed in the groups treated with CDX+RGD-functionalized liposomes loaded with a single fluorescent dye. Conversely, CDX+RGD-functionalized liposomes loaded with 3D demonstrated visible FRET fluorescence and localized inside tumor tissue and inside or outside of tumor blood vessels, indicating that some of intact liposomes had traversed the BBTB *in vivo* (Fig. 10). The microscopic results were consistent with those of *ex vivo* imaging. To further confirm that the liposomes were integrated, DiD was excited at 633 nm and results revealed that it colocalized with FRET fluorescence (Supplementary Information Fig. S10), suggesting that the liposomes were indeed integrated. Similar results were confirmed in the disk-treated groups (Fig. 10, and Supplementary Information Figs. S9 and S10).

4. Discussion

Nano-drug delivery systems such as liposomes have demonstrated excellent properties in the therapy of central nervous system diseases. However, the question as to whether they remain intact during transfer across the BBB and BBTB is unresolved.

FRET is a well-established method to study biological process including biomolecular interactions, protein dynamics and protein conformations[34,35]. Recently, the loading of FRET fluorescence pairs in micelles,[26,36,37]. lipid nanodroplets[38]. and polymer-based nanoparticles[39–41]. was used to investigate the stability of these particles in blood, their internalization in cells, and their mechanism of release[26,27,37,39,40]. However, there are still very few reports concerning the use of the FRET method for exploring the possibility of nano-drug delivery systems (especially liposomes or lipid disks) crossing the BBB and BBTB as intact forms.

In this context, we adopted the FRET tool to explore the stability of liposomes and disks during BBB and BBTB transfer both *in vitro* and *in vivo*. We designed a two-step FRET-effect nano-drug delivery system. DiO, DiI and DiD were simultaneously encapsulated into liposomes or lipid disks. Owing to the presence of FRET from DiO to DiI and DiI to DiD, once excited at 488 nm, a strong DiD fluorescence would be detectable. When they were dissociated, DiD fluorescence would disappear. The presence or absence of DiD fluorescence could then be considered as a reliable indicator of nanoparticle integrity. They exhibited low background signals and little crosstalk between donor (DiO) and acceptor (DiD) as compared to previously reported nanoparticles[26,42].

When considering the integrity of liposomes and disks traversing BBB and BBTB *in vitro*, their stability in cells should be first evaluated. As shown herein, liposomes and disks could be internalized into BCECs and HUVECs and were present as their intact forms. DiD excitation fluorescence was detected and colocalized with the FRET signal, which further confirms that liposomes and disks could be integrated into BBB and BBTB cells. Integrated liposomes or disks crossed the BBB and BBTB with different efficiencies. For instance, Integrated CDX–LS/3D could cross the BBB with the ratio of 0.68‰ at 3 h, which was lower than previous reported[17]. Nonetheless, this indicated that liposomes could traverse the BBB as an intact form.

Appropriate nano-drug delivery systems necessarily must retain their integrity when used in a living biological system, and especially when traversing BBB and BBTB. Here, similar to cell studies, a FRET effect was used to assess the fate of liposomes and disks after systemic administration to normal ICR mice and nude mice bearing an intracranial glioma. *Ex vivo* imaging demonstrated that ligand-containing liposomes or disks could cross the BBB and BBTB as intact forms, which was further confirmed by immunohistochemical studies. This may partially explain the enhanced therapeutic effect of nano-drug delivery systems in central nervous system diseases such as glioma[13,17,22,23].

5. Conclusions

In summary, we have designed two-step FRET-monitored nano-drug delivery systems (liposomes/3D and disks/3D). Once they were dissociated, FRET interactions between co-encapsulated donors and acceptors would be disrupted and DiD fluorescence would disappear. The presence or absence of DiD fluorescence would be an indicator of nano-drug delivery system integrity. Using the above method, we found that liposomes and disks were present in BBB and BBTB cells at least partially as intact particles. *In vivo* experiments also suggested that liposomes and disks could cross the BBB and BBTB *in vivo* as intact forms. This may explain in part the mechanism by which nano-drug delivery systems enhance therapeutic efficacy in the treatment of glioma.

Acknowledgments

We would like to thank the National Center for Protein Science Shanghai for our cryo-EM experiment. This work was supported by China Postdoctoral Science Foundation Grant (No.

2017M611464), National Basic Research Program of China (973 Program, No. 2013CB932500), National Natural Science Foundation of China (Nos. 81773657, 81690263 and 81473149), Shanghai Education Commission Major Project (2017-01-07-00-07-E00052) and Shanghai International Science and Technology Cooperation Project (No. 16430723800).

Appendix A. Supporting information

Supplementary data associated with this article can be found in the online version at http://dx.doi.org/10.1016/j.apsb.2018.01.004.

References

1 Pardridge WM. Blood–brain barrier delivery. *Drug Discov Today* 2007;**12**:54–61.
2 Pardridge WM. Drug transport across the blood–brain barrier. *J Cereb Blood Flow Metab* 2012;**32**:1959–72.
3 Pardridge WM. Molecular Trojan horses for blood–brain barrier drug delivery. *Curr Opin Pharmacol* 2006;**6**:494–500.
4 Ningaraj NS, Rao M, Hashizume K, Asotra K, Black KL. Regulation of blood–brain tumor barrier permeability by calcium-activated potassium channels. *J Pharmacol Exp Ther* 2002;**301**:838–51.
5 Zhan C, Lu W. The blood–brain/tumor barriers: challenges and chances for malignant gliomas targeted drug delivery. *Curr Pharm Biotechnol* 2012;**13**:2380–7.
6 Wei X, Chen X, Ying M, Lu W. Brain tumor-targeted drug delivery strategies. *Acta Pharm Sin B* 2014;**4**:193–201.
7 Kumar P, Wu H, McBride JL, Jung KE, Kim MH, Davidson BL, et al. Transvascular delivery of small interfering RNA to the central nervous system. *Nature* 2007;**448**:39–43.
8 Son S, Hwang DW, Singha K, Jeong JH, Park TG, Lee DS, et al. RVG peptide tethered bioreducible polyethylenimine for gene delivery to brain. *J Control Release* 2011;**155**:18–25.
9 Xin H, Sha X, Jiang X, Zhang W, Chen L, Fang X. Anti-glioblastoma efficacy and safety of paclitaxel-loading Angiopep-conjugated dual targeting PEG-PCL nanoparticles. *Biomaterials* 2012;**33**:8167–76.
10 Wei X, Zhan C, Chen X, Hou J, Xie C, Lu W. Retro-inverso isomer of angiopep-2: a stable D-peptide ligand inspires brain-targeted drug delivery. *Mol Pharm* 2014;**11**:3261–8.
11 Demeule M, Régina A, Ché C, Poirier J, Nguyen T, Gabathuler R, et al. Identification and design of peptides as a new drug delivery system for the brain. *J Pharmacol Exp Ther* 2008;**32**:1064–72.
12 Shen J, Zhao Z, Shang W, Liu C, Zhang B, Zhao L, et al. Ginsenoside Rg1 nanoparticle penetrating the blood–brain barrier to improve the cerebral function of diabetic rats complicated with cerebral infarction. *Int J Nanomed* 2017;**12**:6477–86.
13 Wei X, Gao J, Zhan C, Xie C, Chai Z, Ran D, et al. Liposome-based glioma targeted drug delivery enabled by stable peptide ligands. *J Control Release* 2015;**218**:13–21.
14 Ohgaki H, Kleihues P. Genetic pathways to primary and secondary glioblastoma. *Am J Pathol* 2007;**170**:1445–53.
15 Gotti C, Clementi F. Neuronal nicotinic receptors: from structure to pathology. *Prog Neurobiol* 2004;**74**:363–96.
16 Lindstrom JM. Nicotinic acetylcholine receptors of muscles and nerves: comparison of their structures, functional roles, and vulnerability to pathology. *Ann N Y Acad Sci* 2003;**998**:41–52.
17 Wei X, Zhan C, Shen Q, Fu W, Xie C, Gao J, et al. A D-peptide ligand of nicotine acetylcholine receptors for brain-targeted drug delivery. *Angew Chem Int Ed* 2015;**54**:3023–7.
18 Zhan C, Li B, Hu L, Wei X, Feng L, Fu W, et al. Micelle-based brain-targeted drug delivery enabled by a nicotine acetylcholine receptor ligand. *Angew Chem Int Ed* 2011;**50**:5482–5.
19 Brooks PC, Clark RA, Cheresh DA. Requirement of vascular integrin $\alpha_v\beta_3$ for angiogenesis. *Science* 1994;**264**:569–71.
20 Chandra Kumar C, Armstrong L, Yin Z, Malkowski M, Maxwell E, Ling H, et al. Targeting integrins $\alpha_v\beta_3$ and $\alpha_v\beta_5$ for blocking tumor-induced angiogenesis. In: Maragoudakis ME, editor. *Angiogenesis: From the Molecular to Integrative Pharmacology*. Boston, MA: USA: Springer; 2000. p. 169–80.
21 Belhadj Z, Ying M, Xie C, Hu X, Zhan C, Wei X, et al. Design of Y-shaped targeting material for liposome-based multifunctional glioblastoma-targeted drug delivery. *J Control Release* 2017;**255**:132–41.
22 Zhao X, Chen R, Liu M, Feng J, Chen J, Hu K. Remodeling the blood–brain barrier microenvironment by natural products for brain tumor therapy. *Acta Pharm Sin B* 2017;**7**:541–53.
23 Huang M, Hu M, Song Q, Song H, Huang J, Gu X, et al. GM1-modified lipoprotein-like nanoparticle: multifunctional nanoplatform for the combination therapy of Alzheimer's disease. *ACS Nano* 2015;**9**:10801–16.
24 Lainé AL, Gravier J, Henry M, Sancey L, Béjaud J, Pancani E, et al. Conventional versus stealth lipid nanoparticles: formulation and *in vivo* fate prediction through FRET monitoring. *J Control Release* 2014;**188**:1–8.
25 Jares-Erijman EA, Jovin TM. FRET imaging. *Nat Biotechnol* 2003;**21**:1387–95.
26 Chen H, Kim S, Li L, Wang S, Park K, Cheng JX. Release of hydrophobic molecules from polymer micelles into cell membranes revealed by Förster resonance energy transfer imaging. *Proc Natl Acad Sci U S A* 2008;**105**:6596–601.
27 Lu J, Owen SC, Shoichet MS. Stability of self-assembled polymeric micelles in serum. *Macromolecules* 2011;**44**:6002–8.
28 Yan Z, Wang F, Wen Z, Zhan C, Feng L, Liu Y, et al. LyP-1-conjugated PEGylated liposomes: a carrier system for targeted therapy of lymphatic metastatic tumor. *J Control Release* 2012;**157**:118–25.
29 Gao J, Xie C, Zhang M, Wei X, Yan Z, Ren Y, et al. RGD-modified lipid disks as drug carriers for tumor targeted drug delivery. *Nanoscale* 2016;**8**:7209–16.
30 Gong M, Zhu H, Zhou J, Yang C, Feng J, Huang X, et al. Cryo-electron microscopy study of insect cell-expressed enterovirus 71 and coxsackievirus A16 virus-like particles provides a structural basis for vaccine development. *J Virol* 2014;**88**:6444–52.
31 Zhang P, Hu L, Wang Y, Wang J, Feng L, Li Y. Poly(ε-caprolactone)-block-poly(ethyl ethylene phosphate) micelles for brain-targeting drug delivery: *in vitro* and *in vivo* valuation. *Pharm Res* 2010;**27**:2657–69.
32 Khodarev NN, Yu J, Labay E, Darga T, Brown CK, Mauceri HJ, et al. Tumour-endothelium interactions in co-culture: coordinated changes of gene expression profiles and phenotypic properties of endothelial cells. *J Cell Sci* 2003;**116**:1013–22.
33 Zhu S, Qian L, Hong M, Zhang L, Pei Y, Jiang Y. RGD-modified PEG-PAMAM-DOX conjugate: *in vitro* and *in vivo* targeting to both tumor neovascular endothelial cells and tumor cells. *Adv Mater* 2011;**23**:H84–9.
34 Fruhwirth GO, Fernandes LP, Weitsman G, Patel G, Kelleher M, Lawler K, et al. How Förster resonance energy transfer imaging improves the understanding of protein interaction networks in cancer biology. *ChemPhysChem* 2011;**12**:442–61.
35 Sahoo H. Förster resonance energy transfer-A spectroscopic nanoruler: principle and applications. *J Photochem Photobiol C Photochem Rev* 2011;**12**:20–30.
36 Chen H, Kim S, He W, Wang H, Low PS, Park K, et al. Fast release of lipophilic agents from circulating PEG-PDLLA micelles revealed by *in vivo* Förster resonance energy transfer imaging. *Langmuir* 2008;**24**:5213–7.
37 Chen KJ, Chiu YL, Chen YM, Ho YC, Sung HW. Intracellularly monitoring/imaging the release of doxorubicin from pH-responsive nanoparticles using Förster resonance energy transfer. *Biomaterials* 2011;**32**:2586–92.
38 Klymchenko AS, Roger E, Anton N, Anton H, Shulov I, Vermot J, et al. Highly lipophilic fluorescent dyes in nano-emulsions: towards bright non-leaking nano-droplets. *RSC Adv* 2012;**2**:11876–86.

39 Jiwpanich S, Ryu JH, Bickerton S, Thayumanavan S. Noncovalent encapsulation stabilities in supramolecular nanoassemblies. *J Am Chem Soc* 2010;**132**:10683–5.

40 Ryu JH, Chacko RT, Jiwpanich S, Bickerton S, Babu RP, Thayumanavan S. Self-cross-linked polymer nanogels: a versatile nanoscopic drug delivery platform. *J Am Chem Soc* 2010;**132**:17227–35.

41 Gravier J, Sancey L, Hirsjärvi S, Rustique E, Passirani C, Benoît JP, et al. FRET imaging approaches for *in vitro* and *in vivo* characterization of synthetic lipid nanoparticles. *Mol Pharm* 2014;**11**:3133–44.

42 Gaudin A, Tagit O, Sobot D, Lepêtre-Mouelhi S, Mougin J, Martens TF, et al. Transport mechanisms of squalenoyl-adenosine nanoparticles across the blood–brain barrier. *Chem Mater* 2015;**27**:3636–47.